Sādhanā (2020)45:116
https://doi.org/10.1007/s12046-020-01352-y

An efficient miniature air suction system for chemical sensors for micro air vehicle application

M D DESHPANDE[1], M SIVAPRAGASAM[2,*] and S UMESH[2]

[1]Formerly, M S Ramaiah University of Applied Sciences, Bengaluru 560 058, India
[2]Department of Aerospace Engineering, Faculty of Engineering and Technology, M S Ramaiah University of Applied Sciences, Bengaluru 560 058, India
e-mail: sivapragasam.aae.et@msruas.ac.in

MS received 25 May 2017; revised 23 March 2020; accepted 26 March 2020

Abstract. This paper describes the design of a miniature air suction system to house a chemical sensor. It has been designed to improve the aerodynamic chemical sensing efficiency and to have a low weight since it is meant to be mounted on a micro air vehicle. The design is done around a readily available miniature axial flow fan by computational methods. A converging-diverging shape for the air suction system with the sensor disc having a central hole and mounted at the throat is proposed as good design concept. The systematic approach has led to a light weight system with high aerodynamic efficiency even under extreme flow conditions that may be caused by MAV manoeuvre or cross winds.

Keywords. Chemical sensing; micro air vehicle; air suction system; miniature axial flow fan; aerodynamic efficiency; Reynolds analogy.

1. Introduction

Detection of poisonous chemical gases, emanating in small traces either from hidden storage chambers or from landmines, requires highly sensitive chemical sensing devices. The devices, if made small and light, can be mounted on a micro air vehicle (MAV) and ferried to the suspected site of the air to be sensed. This requires, amongst other things, a high aerodynamic efficiency of sensing a gas. The miniature chemical sensors employed in such devices require the gas-laden air from the surroundings to be 'breathed in' and directed to the sensors. An air suction system, incorporating a suction fan, is thus required to suck the surrounding air and direct the air to the chemical sensor.

It is important to understand the differences between the aerodynamics of gas and aerosol sampling [1] since the principles involved are not the same. Different chemical sensing missions will have varied requirements. These should be clearly recognised and respective specifications drawn, and a proper chemical sensor identified so that design of the miniature air suction system can be done effectively. Chemical sensing missions involving particulate material will require a different design strategy [2, 3]. They can be addressed with the experience gained from the present research work.

We can learn from the animal world and olfactory flows, especially from a dog, since the dog's nose is recognized as the gold standard of olfactory acuity [4]. However, in this biomimicry exercise, a keen observation, intelligent imitation and scaling are required since each sampling mission has its own peculiarities. When dogs are trying to detect the landmines for explosive vapour, they are known to actually kick up dust by blowing air from the outer parts of their nostrils so that these dust particles are sucked in during inhalation [5]. However, a suction process is not directionally efficient as it is known from potential flow theory that a sink flow cannot be vectored. Hence, most of the inhaled air is extraneous if the nose stand-off distance from the ground or source is large. This brings in an inherent difficulty in both the cases, either inhaling a vapour or the aerosols.

Mounting the sensor device on a MAV has the advantage that the sensor can be taken closer to the suspected sample and to survey large areas at relatively high speeds, a requirement in gas leakage accidents [6]. Chemical sensors often suffer from having a slow response time and this becomes a major handicap when measurements are to be made at low concentration levels. Further, many sensors have short duration of their applicability when measurements can be done [7]. To overcome this difficulty either one should enhance the sensor properties or the measurement conditions [8]. All these point to the need of an efficient air suction system so that the chemical sensor sensing efficiency is improved.

A key step in the gas sensing process is the diffusion of target gas molecules onto the surface of the sensing layer

*For correspondence
Published online: 11 May 2020

[9]. The response of the sensor depends on the concentration gradient across the sensing element. This fact prompted us to use the Reynolds analogy. Since mass, momentum and energy transfers are related by similar transport processes and governing equations, a high mass transfer also means a high momentum and energy transfer. The diffusion flux being driven by the concentration gradient is analogous to the momentum and heat fluxes driven by velocity and temperature gradients, respectively [10, 11].

Micro-electro-mechanical-systems (MEMS)-based technology is used to design and fabricate miniature chemical sensors that have good performance characteristics like fast response, high sensitivity and low power consumption [12]. Of the several types of chemical sensors, metal oxide (MOX) sensors are popular and many commercial sensors are available. For example, ams AG CCS811 (detects CO_2, volatile organic compounds (VOC)), Bosch Sensortec BME680 (VOC), Figaro TGS8100 (H_2, C_2H_5OH) and Sensirion SGPC2 (VOC) are commercially available. Recently, Micralyne introduced MOX sensors as small as 1 mm × 1 mm. The thickness of these sensors is typically 1 mm or less.

The present study is meant for sampling a gas or vapour and not for aerosols or particles. Since the sensor is to be mounted on a MAV, weight and power requirements become crucial design parameters. A sensor element in the form of a thin-film and typically 1 mm × 1 mm size is assumed. A sensor disc of 10 mm diameter is selected so that several such sensor elements can be fixed on one side of this disc facing the flow. A miniature axial flow fan is an important and integral component of the air suction system. Use of a fan in the air suction system has an advantage compared to the biological systems or the systems where the collection of the chemical sample is done by the forward motion of the vehicle. The presence of a fan makes it possible that the MAV on which the sensor is mounted can go and perch or hover on a suspected chemical source like a landmine and sniff air for sensing.

Miniature axial flow fans are readily available since they are extensively used for cooling of PCBs, CPUs and high capacity USB drives. The conventional large fans are designed based on the basic aerodynamic and turbomachinery principles which are well documented [13–15]. However, the miniature fans in the present study operate at low Reynolds numbers typifying highly viscous flow and low aerodynamic efficiency. Higher fan efficiency implies higher mission duration owing to less power drawn from the batteries powering the drive motor. The deterioration in fan performance at low Reynolds numbers is well documented and some studies have been published concerning low Reynolds number turbomachinery [16–21]. We tested the performance of such miniature fan and built the remaining flow system around this fan for high efficiency.

The present paper is organised as follows. We first select a miniature axial flow fan for the air suction system. The computational procedure for evaluating the fan performance characteristics is detailed next. Two air suction duct concepts are presented and one is selected by resorting to Reynolds analogy. Further, results are presented for optimising the selected air suction duct such that its aerodynamic performance is enhanced and its weight is minimal. The performance of the optimised air suction duct is also studied in real flight situation through computations at different flight velocities and angles of attack. In the final section conclusions are provided.

2. Fan selection for air suction system

A miniature fan is selected which has the credentials regarding weight, power and performance criteria so that it can be used in the present air suction system. For this purpose a miniature axial flow fan (model UF3H3, Sunon, Taiwan, see figure 1) having a rotor diameter of 16 mm, weighing 1.28 grams and requiring only about 0.1 W power is selected. We performed computations to evaluate the performance of the UF3H3 fan and accepted it, and around this fan the present air suction system is designed to achieve a high aerodynamic sensing efficiency.

These steps will be elaborated in the following sections and explained especially how the design of a near optimum air suction system which has the unique features to have high aerodynamic sensing efficiency is achieved. If there are several sensing elements side by side their sensing efficiency should be retained high for all flight conditions. This becomes important if there is a flow angularity due to different flight direction of the MAV or due to cross wind. In extreme cases the flow may separate in the duct and the recirculating air mass may make the sensors less effective. Also in the wake of the fan hub there is a reverse flow. It will be seen how the present design handles these situations effectively.

Figure 1. Sunon model UF3H3 miniature axial flow fan (www.sunon.com). The fan rotor diameter is 16 mm and the casing size is 17 × 17 × 3 mm.

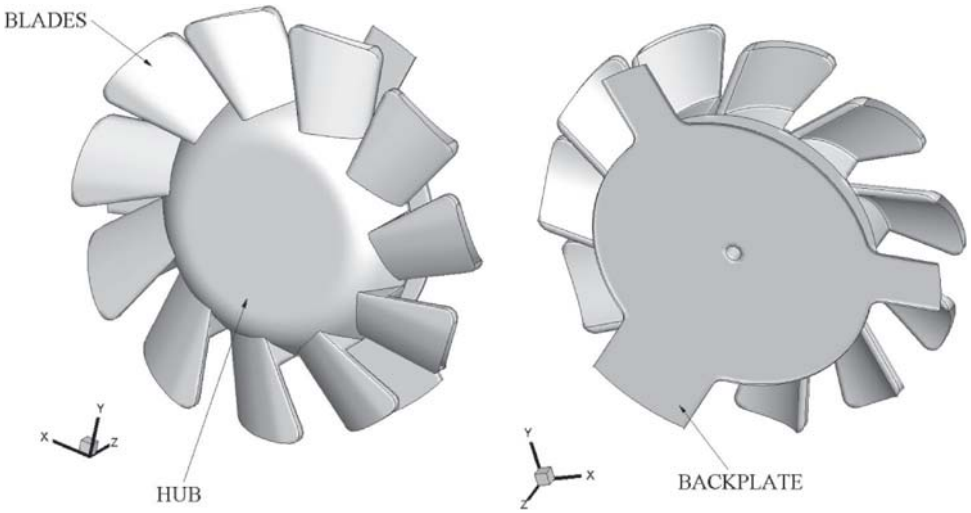

Figure 2. Geometry of Sunon UF3H3 fan. The eleven blades can be seen in the figure on the left and the back plate on the right.

3. Computation of Sunon UF3H3 fan performance

We did computations to evaluate the performance of the UF3H3 fan. The Navier-Stokes equations were solved numerically using the CFD solver ANSYS Fluent. The flow field was assumed to be steady, incompressible and laminar. The convective terms in the Navier–Stokes equations were discretised by a second-order upwind scheme and the viscous terms by a second-order central differencing scheme. All calculations were done in double-precision arithmetic. The convergence of the residuals was 10^{-5}. The computational geometry for the UF3H3 fan included the back plate with struts which are located behind the fan and serves to support the fan to its casing. We have included this back plate in the computations as it is an integral part of the fan along with the casing and had to be mounted in the miniature air suction system as a single entity. The fan with eleven blades and the back plate is shown in figure 2.

The computational domain was a circular cylinder whose diameter was $2D$; D is the rotor diameter of the fan. The length of this domain extended up to $3D$ from the inlet of the fan and $5D$ from the exit of the fan. The origin of the computational domain was fixed at the upstream face of the fan hub at $(x, y, z) = (0, 0, 0)$, with the flow being along z. At the inlet of the computational domain total pressure boundary condition was imposed, and at the outlet the static pressure was specified. The outlet static pressure was varied to obtain the required inlet flow rate. The no-slip boundary condition was specified on the fan blades, hub, back plate, and the walls bounding the computational domain. The fan speed was 13,000 rpm. The Reynolds number (Re) based on blade mid-span rotational velocity and chord length at blade mid-span was 1791. The Re defined in this manner is independent of the fan operating point for the given rpm [16].

An unstructured grid system with tetrahedral cells was used to generate the computational grid within the flow domain. It was ensured that there were fine grid cells near the fan blades, hub and back plate. The number of grid points for the computations were chosen after a careful grid independence study. We had earlier experience of performing computations with the ebm-papst model 252 N, Germany, miniature axial flow fan [22]. For this fan we had performed a grid independence study with 496,348 (coarse), 913,493 (medium) and 1,383,736 (fine) grid points. The fan performance characteristics, in terms of its pressure rise versus volumetric flow rate were found to be convincingly grid independent. Further, the Grid Convergence Index (GCI) for the discretisation error [23] indicated that the medium grid was quite adequate. Based on this experience a computational grid with 902,950 grid points was chosen for the Sunon UF3H3 fan.

3.1 *Fan performance characteristics*

The Sunon UF3H3 fan performance characteristics from the present computations is plotted in figure 3 along with the data specified in the manufacturer's technical specifications. It may be noted that the agreement is good particularly in the nominal operating range of the fan. However, the present computations predict a higher pressure rise in the stalled region of operation of the fan.

3.2 *Velocity distribution*

The vectors of axial (z-component) velocity at a longitudinal plane are shown in figure 4. It is seen that a reverse flow region exists behind the fan hub. This region extends

to a significant region behind the hub. This is an important observation because the placement of the chemical sensor becomes crucial. The sensor cannot be located in this reverse flow region since its sensitivity will be hampered. The ideal positioning of the chemical sensor would be downstream of this reverse flow region. Further, a converging- diverging arrangement will be employed in the actual duct designed to counteract this difficulty and have a high velocity flow around the chemical sensor to increase mass transfer.

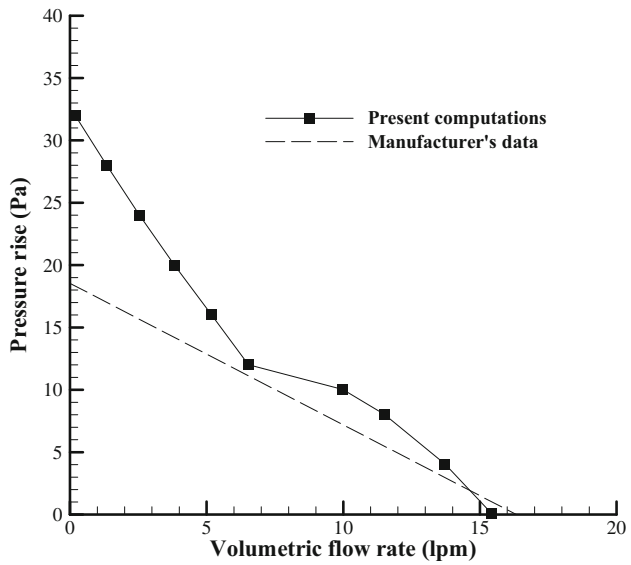

Figure 3. Sunon UF3H3 fan computational performance compared with manufacturer data. The fan speed is 13,000 rpm.

4. Air suction duct design concepts

Use of a fan in the sampler duct has an advantage compared to the biological systems or the systems where the collection of the chemical sample is done by the forward motion of the vehicle. We are free to use all the air sucked inside the sensor duct for olfactory purpose unlike even in the case of a dog nose where only a small fraction of the inhaled air is used for this purpose. Of course, the high sensitivity of the olfactory area in case of a dog or similar cases makes sensing very efficient.

Based on these requirements and design constraints, we arrived at two concepts, Concept 1 and Concept 2, as illustrated in figure 5. In Concept 1, the chemical sensor disc is behind the fan whereas it is in front of the fan in Concept 2. The duct additions in front of the fan in Concept 1, and behind the fan in Concept 2 are for computational convenience and can be discarded later to reduce the weight. The chemical sensor elements are to be fixed on a disc which is located at the throat of the converging-diverging duct so that the chemical mass transfer from air to the sensing element is made high.

In Concept 1 the sensor disc is located behind the fan and we have verified for figure 5(a) that this location is downstream of the flow reversal region. In Concept 2 the sensor disc is located ahead of the fan. In the absence of the present velocity plot (figure 4) and detailed knowledge of the flow separation, Concept 1 would have appeared a natural choice. It was probably because of the aerodynamic observation that a jet (from a fan here) can be more directed than any suction device (again the same fan, but the upstream side) which sucks the air from all directions and hence is less pointed. This should result in a poor

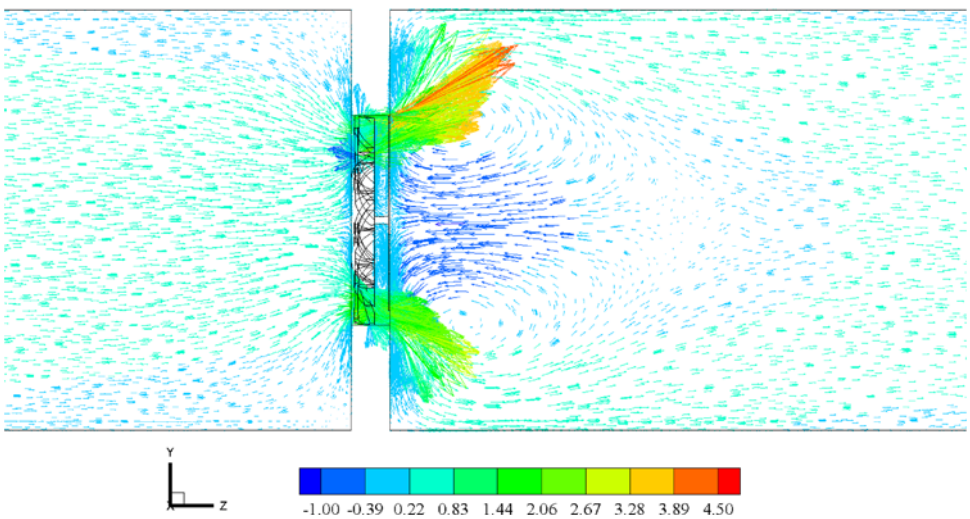

Figure 4. Vectors of axial velocity (m/s) in a longitudinal plane shown close to the fan. Volumetric flow rate = 11.5 lpm and pressure rise = 8.03 Pa. Notice the large reversed flow region (with negative velocity) behind the fan. The chemical sensor should *not* be positioned here.

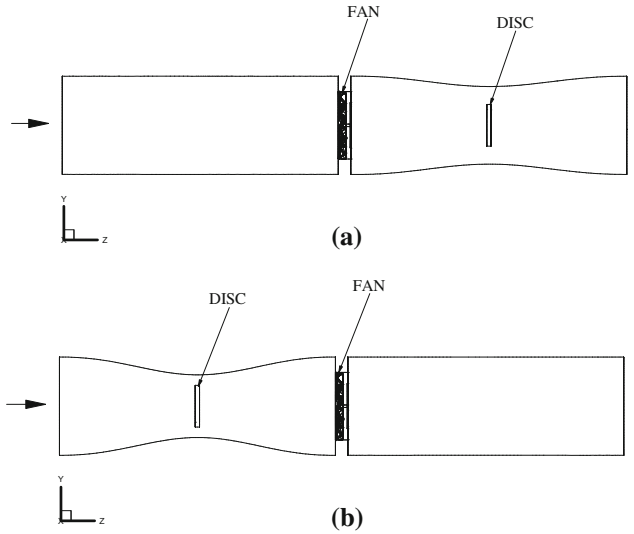

Figure 5. Two concepts developed for placing the sensor disc. (a) Concept 1 where the sensor disc is located behind the fan. (b) Concept 2 where the sensor disc is located ahead of the fan. The flow is from left to right in both the concepts.

aerodynamic sensing efficiency of the sensor for Concept 2 compared to that for Concept 1. But it will be seen that due to the separated flow behind the fan hub and also by a careful design of the duct geometry and the sensor disc location, Concept 2 turns out to be superior to Concept 1. Consequently, Concept 2 is chosen and we give below the details of this selection procedure.

In both the concepts the disc where the chemical sensor is to be affixed is kept at the throat of a converging-diverging duct so that the chemical mass transfer from air to the sensing element is made high. The diameter of the sensor disc was chosen to be 10 mm. The converging-diverging duct was of sinusoidal profile in the preliminary comparative study. Once one of the two concepts is finalised a more careful design of shape and size of the duct is made later through computations.

Now, computations were performed for the two concepts shown in figure 5 and the fan performance results are plotted in figure 6. In figure 6(a), Concept 1 is seen to be a little superior to Concept 2 especially at high flow rates. But this advantage is only marginal in the operational range of the fan. Shown in this figure are also the system resistance curves obtained by computations in the same manner as detailed earlier but assuming zero fan speed. The intersection point indicates the operating point. We see presently that this point happens to coincide with the maximum efficiency point and also it is sufficiently to the right of the stall region thus assuring any small modification in the design (like adding a protective screen) or eventualities like sudden gusts will not push it into the stall region. We will see in section 7 that optimisation of the flow system will lead to an increased flow rate and further the forward velocity of the MAV will lead

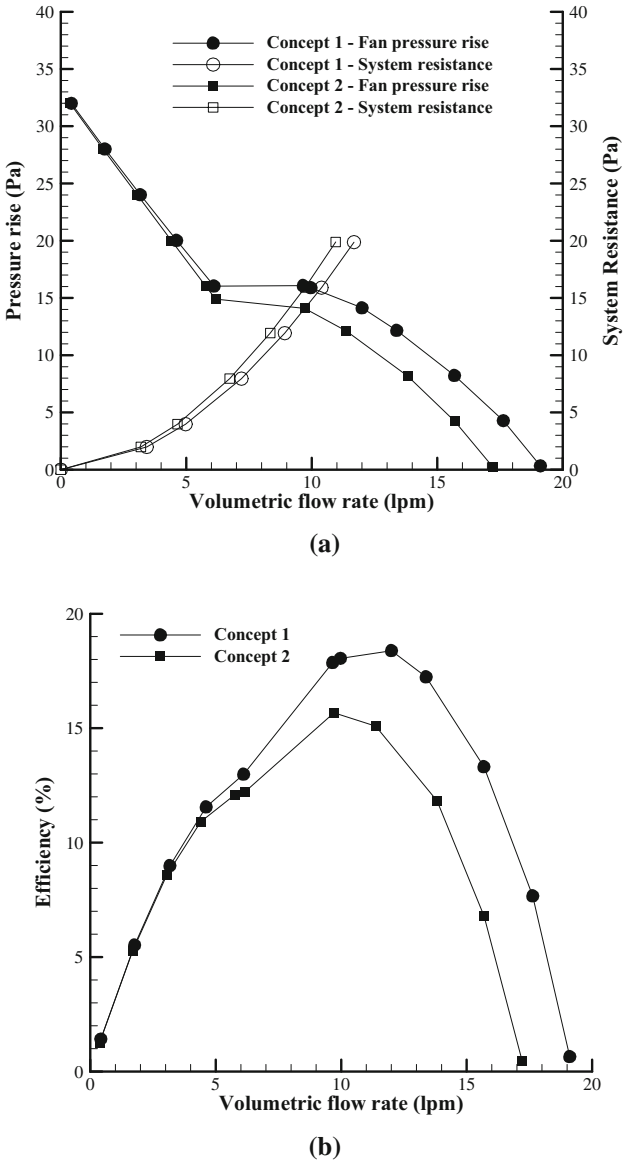

Figure 6. Performance of the fan in the two conceptual duct designs. (a) Pressure rise versus fan's volumetric flow rate along with the system resistance curves and (b) hydrodynamic efficiency of the fan.

to a substantial increase in flow rate without increasing the fan rpm.

In figure 6(b) the hydrodynamic efficiency is defined as,

$$\eta = \frac{Q\,\Delta p}{T\,\omega}$$

where, Q is the volumetric flow rate, Δp is the pressure rise across the fan, T is the torque on the fan blades and hub, and ω is the fan rotational speed. Efficiency η goes to zero at both the ends because either Q goes to zero or Δp goes to zero. The operating point is close to the peak that occurs in between and to the left of this peak the fan gradually starts

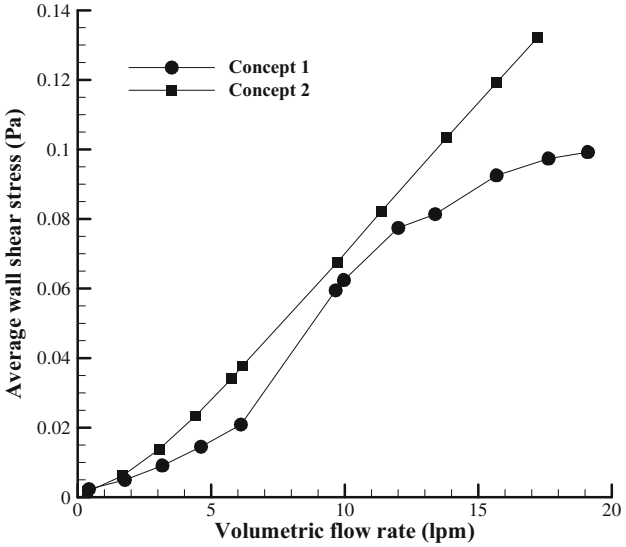

Figure 7. Average values of wall shear stress on the disc where the chemical sensor is to be fixed for the two concepts.

to stall and changes in Q and torque T lead to a decrease in η. Again we see Concept 1 to be superior at high flow rates but only marginally in the range of interest.

It is apparent from figure 6 that the fan performance in Concept 1 is slightly better than that in Concept 2. However, when we evaluated the average wall shear stress (τ_w) on the upstream face of the disc where the chemical sensor is to be fixed we found that the disc in Concept 2 had larger values of average wall shear stress for all flow rates as shown in figure 7.

We had earlier discussed that a high mass transfer from the sampling gas to the chemical sensor can be obtained by achieving a high momentum transfer. It thus becomes clear, from figure 7, that slightly higher τ_w values on the disc can be achieved with Concept 2. As mentioned earlier, Concept 2 has the advantage that there is no danger of the sensor disc being in the separated wake of the fan hub and hence the length of the device can be shortened. Based on these considerations we choose this concept for further design optimisation.

With Concept 2 chosen, the new duct geometry is illustrated in figure 8. This geometry has certain other advantages apart from the ones shown above by CFD simulations. Now the downstream part of the duct can be completely omitted leading to a saving in weight. The fan is protected from the front by the duct. Also, it is possible to design the front part of the duct so that the flow does not separate but remains axisymmetric when the inlet flow is at an angle relative to the axis of the duct due to MAV manoeuvre or due to crosswind. Thus the present choice should enable the whole area of the chemical sensor disc to be exposed well to the gas laden air to be sensed and also the fan to receive a flow that is nearly axisymmetric.

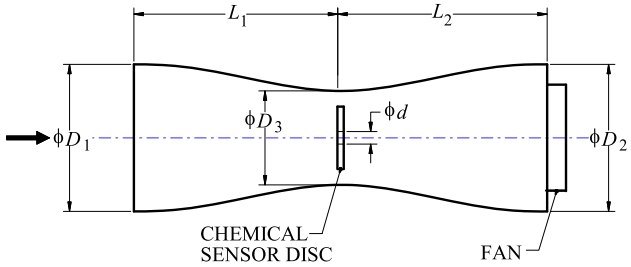

Figure 8. Conceptual air suction duct design for chemical sensor.

5. Optimisation of the air suction system

Now the design of the air suction duct is done around Concept 2 as shown in figure 8. Diameters D_1, D_2 are fixed to be 23.5 mm because of the chosen fan dimensions. The sensor disc diameter is chosen to be 10 mm by practical considerations so that several sensor elements can be fixed on the windward side. It should give sufficient area to fix the sensors. Thickness of this disc is taken to be 1 mm but may be changed if need be without affecting the aerodynamic performance of the system. Further, a hole of diameter d is fashioned at the centre of the disc to enhance the shear stress on the disc which will consequently improve the sensitivity of the chemical sensors. What is required now is to select D_3, L_1, L_2, d and the shape of the duct to have best sensing efficiency and enhanced aerodynamic performance. The convergent portion needs quick acceleration to avoid flow separation in case of cross-flow in front of the front duct. This is done by selecting an elliptic profile with vertical tangent to the profile at entrance and horizontal tangent at the throat. Further, the diverging portion is chosen to be a sinusoidal profile leading to the suction fan so that it has smooth connection at both the ends. The disc is located at the throat of the air suction duct.

Once the major design decisions have been made regarding the shape, the remaining part of the problem amounts to selecting the four dimensions D_3, L_1, L_2 and d to achieve good performance. Also, in this problem there is no simple cost function to be minimised. Selection needs to be done by considering several factors, like, the shear stress on the sensor disc for its magnitude and uniformity of distribution, and the fan performance. Also, four parameters in the problem make it a complex problem since any variation in a parameter to inspect what happens to the performance need solution of the Navier-Stokes equations. Further, the procedure is made more time consuming because for the changed geometry, however small the change, a new grid for computations has to be generated.

Because of these difficulties we do not resort to traditional optimisation methods. Based on our experience and some exploratory studies, a practical strategy was adopted. First, a hierarchy for the order of selection of

Table 1. Geometric parameters considered in the design of the air suction duct.

Geometric Parameter	Trial Values (mm)	Selected value (mm)
d	0, 1, 2, 3	2
D_3	12.5, 14, 15, 17.5	14
L_1	8, 10, 15	10
L_2	15, 20, 25, 30, 35	20

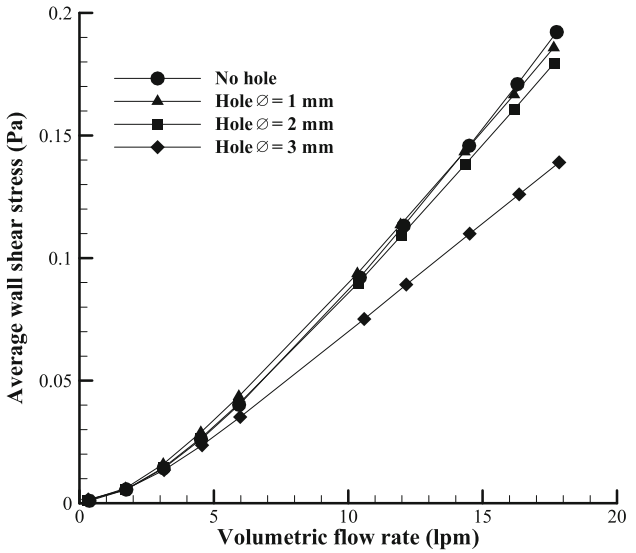

Figure 9. Average wall shear stress on the disc for different hole diameters.

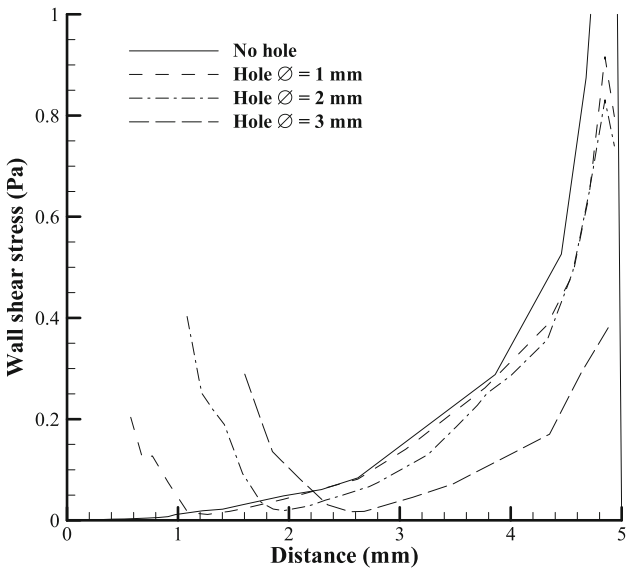

Figure 10. Shear stress distribution on the disc in the radial direction.

the four parameters was fixed to be d, D_3, L_1, L_2. The parameters that have a stronger influence on the outcome were given a higher position to be fixed first. This chosen order was verified by some preliminary

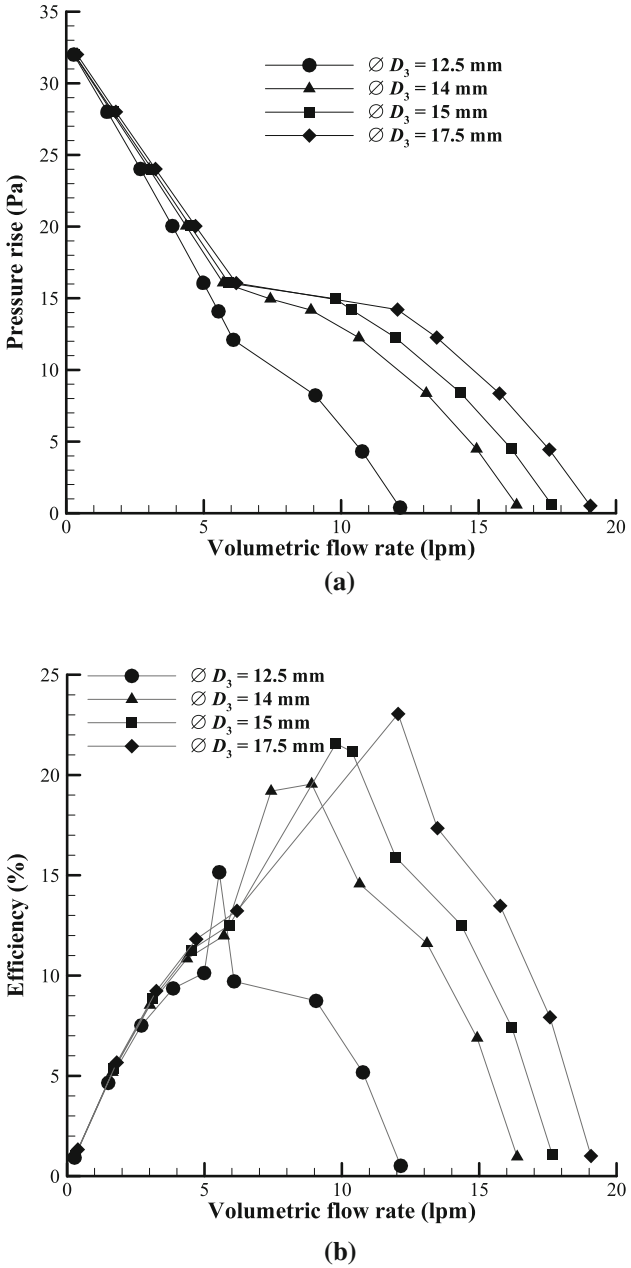

Figure 11. Performance of the fan for different throat diameters D_3. (a) Pressure rise versus fan's flow rate, and (b) hydrodynamic efficiency of the fan.

computations and confirmed further after one round of optimisation by the sensitivity of the performance to the chosen values of the parameters.

The trial values of the parameters chosen for computational studies and the ones which were finally selected are listed in table 1. We give below the details of this selection procedure.

As explained above, the first parameter to be varied and studied was the hole diameter d. Since the sensor disc diameter is 10 mm, d is chosen to cover a wide range, being 1, 2 and 3 mm, with no hole case of $d = 0$ mm being the

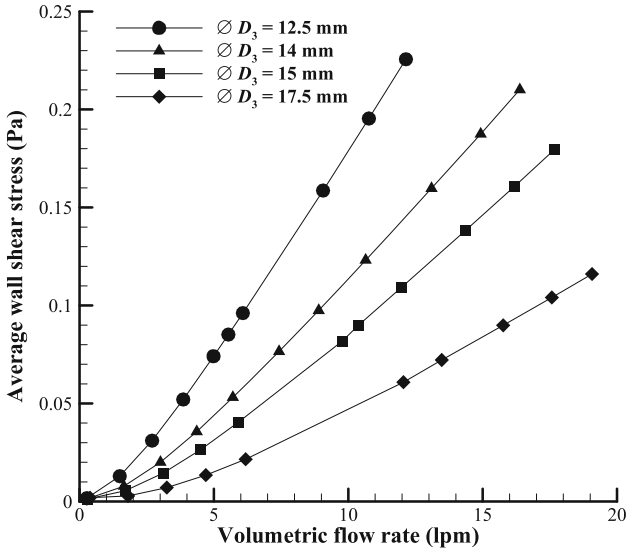

Figure 12. Average wall shear stress on the disc for different throat diameters D_3.

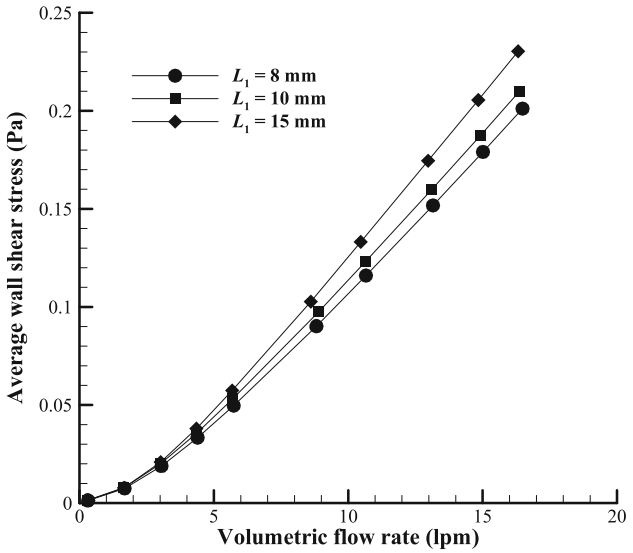

Figure 13. Average wall shear stress on the disc for different lengths of converging section L_1.

basic case for comparison. Computations were performed for these four cases of hole diameters holding other three parameters fixed. The idea here is to see how much the hole diameter d affects the fan performance, average shear stress distribution on the disc front face (where sensor elements are to be fixed, and by Reynolds analogy high shear stress means high mass transfer leading to a good response of the sensors) and the actual distribution of shear stress on the front wall. It may be mentioned that while calculating the average shear stress on the front wall of the sensor disc, two rings of 0.5 mm width one close to the outer edge of the disc and the other around the hole were omitted. This is because of an assumption that the sensor element may not extend to the very edge of the available area.

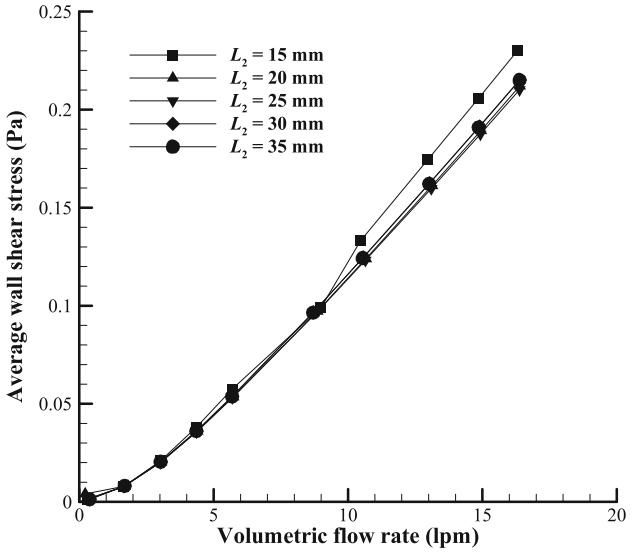

Figure 14. Average wall shear stress on the disc for different lengths of diverging section L_2.

As expected, the diameter of the hole d did not have any significant effect on the performance of the fan. Next we consider the average wall shear stress on the disc which is plotted in figure 9. Again the diameter of the hole does not seem to significantly change the average wall shear stress on the disc except for the disc with a larger hole of 3 mm where the stress values are lower. Even though these three tests to study the influence of d turned out not to indicate any strong bias, we will see the next comparison to give a conclusive choice.

The shear stress distribution on the disc in the radial direction is plotted in figure 10 for the case where the pressure rise is 12 Pa. It is apparent from this figure that the value of shear stress at the centre of the disc is zero for the disc with no hole. In fact, there's a stagnation region of nearly zero shear stress in the middle of the disc. Thus the centre of the disc is not a good location to fix a chemical sensor. For the discs which have a hole, on the other hand, the shear stress peaks near the edge of the hole and the highest value is for the disc with 2 mm diameter hole. There is a minimum value of shear stress in these three curves indicating a stagnation ring, flow being radially inwards inside the ring. The shear stress value actually changes the sign here (not shown in the figure) but is of no consequence for the chemical sensor since the sensing efficiency only depends on the shear stress magnitude. This situation is different from that of a separated region and flow reversal behind a fan as was shown in figure 4 since fresh chemical laden air continuously comes in contact with the sensor in the present case. It should be clear now why the shear stress plot is made for the absolute value only in figures 9 and 10. The effectiveness of the central hole is further demonstrated in section 7. Another peak in the shear stress is found near the rim of the disc. From the hole

at the centre of the disc to the rim the shear stress values are nearly same for the disc without hole and with 1 mm and 2 mm holes. For the disc with 3 mm hole, on the other hand, the shear stress values are lower. Thus we choose the disc with 2 mm hole diameter. Further, a disc with a hole of 2 mm diameter will allow for sufficient space for fixing the chemical sensors.

Now we are in a position to optimise the air suction duct. The remaining three dimensions of the duct, namely the throat diameter (D_3), the length of the converging portion (L_1) and the length of the diverging portion (L_2) are to be optimised individually, one by one, in that order holding d = 2 mm. The fan performance and efficiency and the skin friction on the disc are kept in mind while optimising these values.

The throat diameter D_3 was varied with the following values: 12.5 mm, 14 mm, 15 mm and 17.5 mm. The fan performance characteristics are shown in figure 11 and the average wall shear stress on the disc is shown in figure 12. It can be seen that though the fan performance is better with D_3 = 17.5 mm the skin friction on the disc is lower for this case at all flow rates. The average skin friction on the disc is highest for D_3 = 12.5 mm; however, the fan performance is poor. As a compromise we choose D_3 = 14 mm which has large values of skin friction on the disc and a reasonably good fan performance.

With the throat diameter D_3 chosen as 14 mm, the length of the converging portion of the air suction duct (L_1) can be optimized. The values of L_1 chosen for study are 8 mm, 10 mm and 15 mm. The average wall shear stress on the disc is shown in figure 13. The fan performance is unaffected by the change in L_1, but the average wall shear stress values are high for L_1 = 15 mm. However, using this length of 15 mm will eventually increase the weight of the air suction duct. Thus, we choose L_1 = 10 mm.

With D_3 = 14 mm and L_1 = 10 mm the length of the diverging section of the duct L_2 can be optimized. The values of L_2 chosen for parametric studies are 15 mm, 20 mm, 25 mm, 30 mm and 35 mm. The average wall shear stress on the disc is shown in figure 14. Again, the fan performance is unaffected by the change in L_2, but the average wall shear stress values are slightly high for L_2 = 15 mm. However, using this length of 15 mm will have the fan operating in a disturbed flow due to the disc ahead and hence we choose L_2 = 20 mm.

The final chosen values of air suction duct are given in table 1 and this geometry is shown in figure 15.

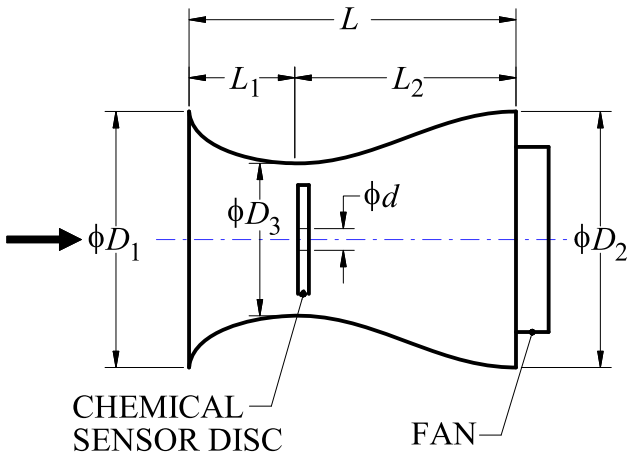

Figure 15. Optimised air suction duct design for chemical sensor. The length of the converging section L_1 = 10 mm, the throat diameter D_3 = 14 mm and the length of the diverging section L_2 = 20 mm. The disc with 10 mm diameter has a central hole of d = 2 mm diameter.

6. Structural consideration and fabrication

After the aerodynamic design of the air suction duct the structural design of this duct was carried out and it has helical ribs as shown in figure 16(a). The thickness of the shell was 1 mm and the thickness and the width of the ribs were 1 mm. Ease and possibilities in fabrication were the deciding factors while deciding the thickness value so that

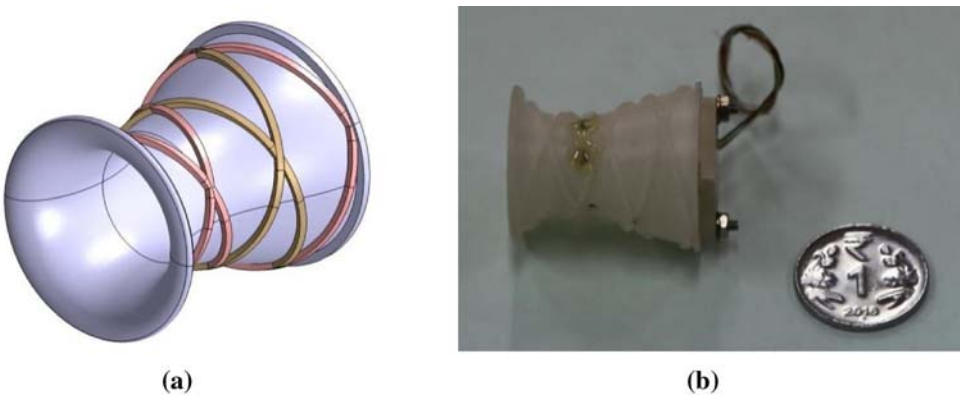

Figure 16. (a) Structural design of air suction duct with helical ribs. (b) Air suction duct fabricated by Rapid Prototyping using ABS plastic material.

Table 2. Summary of the weights (gram).

Item	Weight (gram)
Air Suction Duct	2.226
Sunon Fan Model UF3H3-500	1.283
(Bolt, Nut, Washer) 2 numbers	0.819
Sensor Disc Dummy + 2 studs to fix	0.214
Air Suction System Assembly	4.542 (Total)

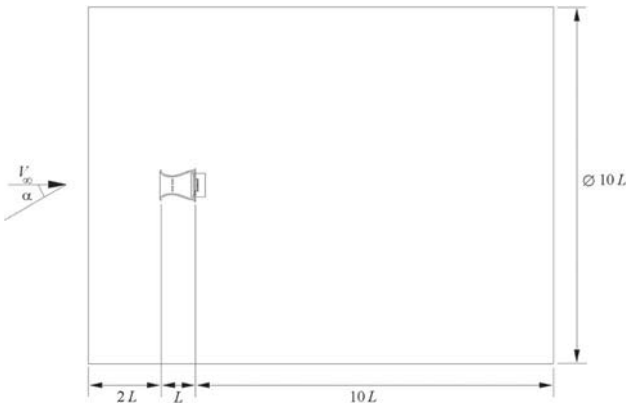

Figure 17. Computational domain to study the effect of free-stream velocity and angle of attack. L = 30 mm.

it can be kept minimum to reduce the weight. Since the fan has two holes of 2 mm diameter in its frame they were used to bolt it to the air suction duct shell. Accordingly four holes were arranged on the diaphragm at the end of the diverging part so that any two diagonal holes can be used for bolting the fan. The air suction duct was fabricated using Rapid Prototyping technology with ABS plastic material for reduced weight. The fabricated duct is shown in figure 16(b). This duct was initially tested in a low-speed wind tunnel, and later mounted on a quad-rotor and flight tested for its structural integrity.

The weights of the individual components of the air suction system are presented in table 2. The weight of the air suction system including the fan is about 4.5 gram. There is scope to reduce the weight without a deterioration of the aerodynamic performance.

7. Performance evaluation in real flight situation

We also studied the performance of the optimised air suction duct at different inlet velocities and at various angles of attack by numerical simulations. We performed computations with the air suction duct enclosed in a larger computational domain shown in figure 17. The computational domain extended two air suction duct lengths ahead of the duct and ten duct lengths downstream. The diameter of the computational domain was ten times the length of the air suction duct. This geometry was chosen such that it

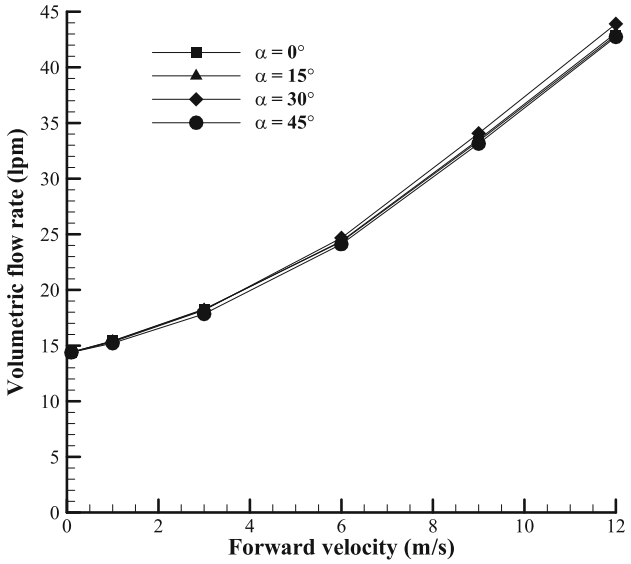

Figure 18. Volumetric flow rate at the inlet of air suction duct at different forward velocities and angles of attack.

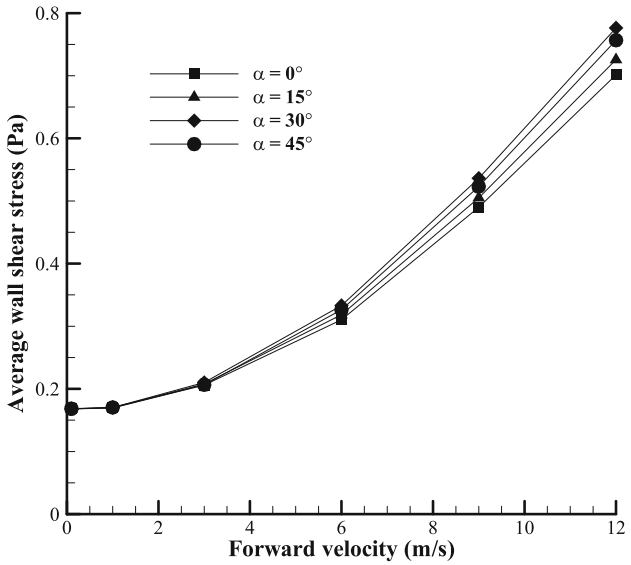

Figure 19. Average skin friction on the disc at different forward velocities and angles of attack.

represents the air suction duct being exposed locally to different velocity fields when mounted on a MAV. The total number of cells for the computations was 1,646,586. The discretisation of the Navier-Stokes equations was done by second-order accurate schemes. At the inlet of the computational domain freestream velocity and the required angle of attack were specified, and pressure-outlet boundary condition was applied at the domain outlet.

Computations were done for different freestream velocities of 0.1 m/s, 1 m/s, 3 m/s, 6 m/s, 9 m/s and 12 m/s and angles of attack 0°, 15°, 30° and 45°. The speed of the fan was held constant at 13,000 rpm. These values were

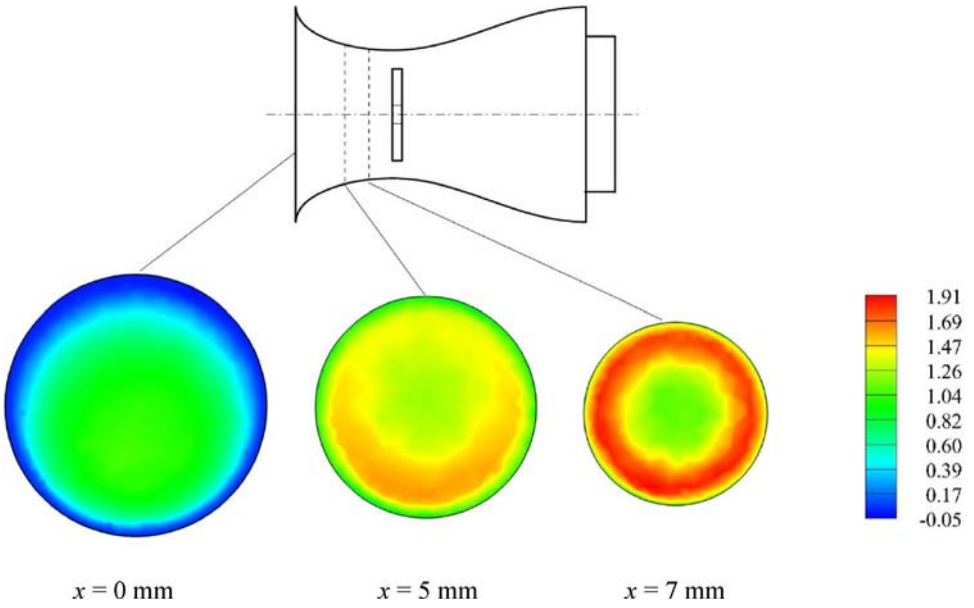

Figure 20. Contours of axial velocity (m/s) at various stations in front of the sensor disc. Sensor disc is at x = 10 mm. Forward velocity = 1 m/s and angle of attack = 45°.

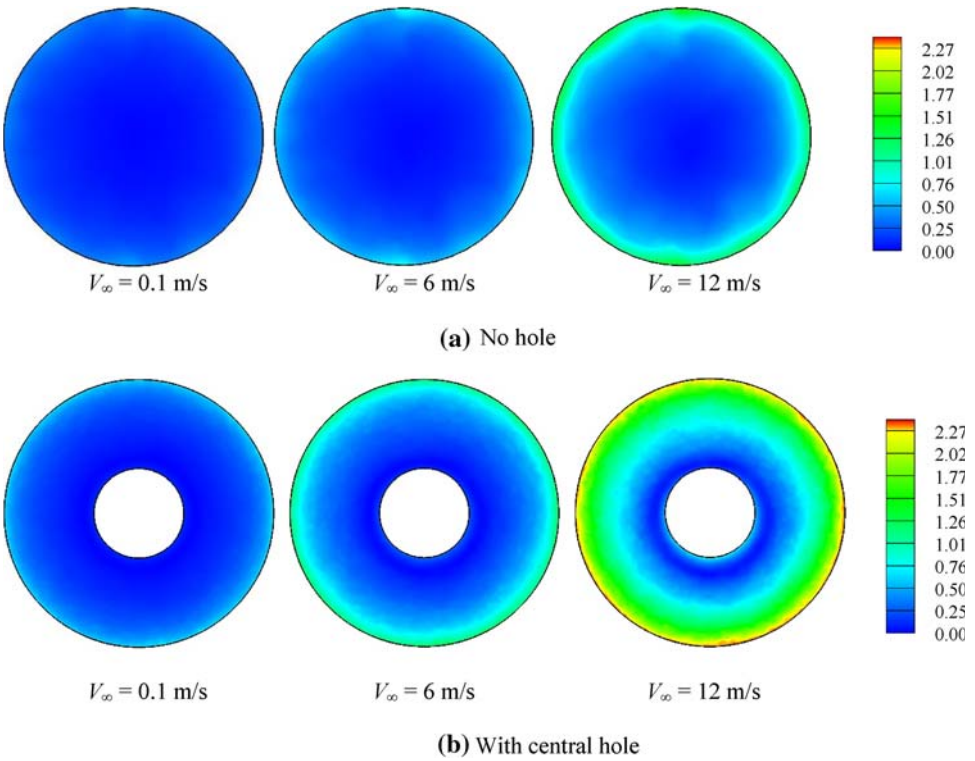

Figure 21. Contours of wall shear stress (Pa) on the sensor disc for different freestream velocities for (a) no hole and (b) with central hole on the sensor disc. The angle of attack is 45° in all these cases.

selected to cover the extreme values that may occur in flight. The results are plotted in figure 18 where the volumetric flow rate evaluated at the inlet of the air suction duct is plotted against different forward velocities. As expected the flow rate increases with an increase in forward velocity but quite interestingly the flow rate does not depend on the angle of attack even for as large an angle as 45°. It indicates that the design of the air suction duct is successful.

The average wall shear stress distribution on the disc is plotted in figure 19. It can be seen that the τ_w values

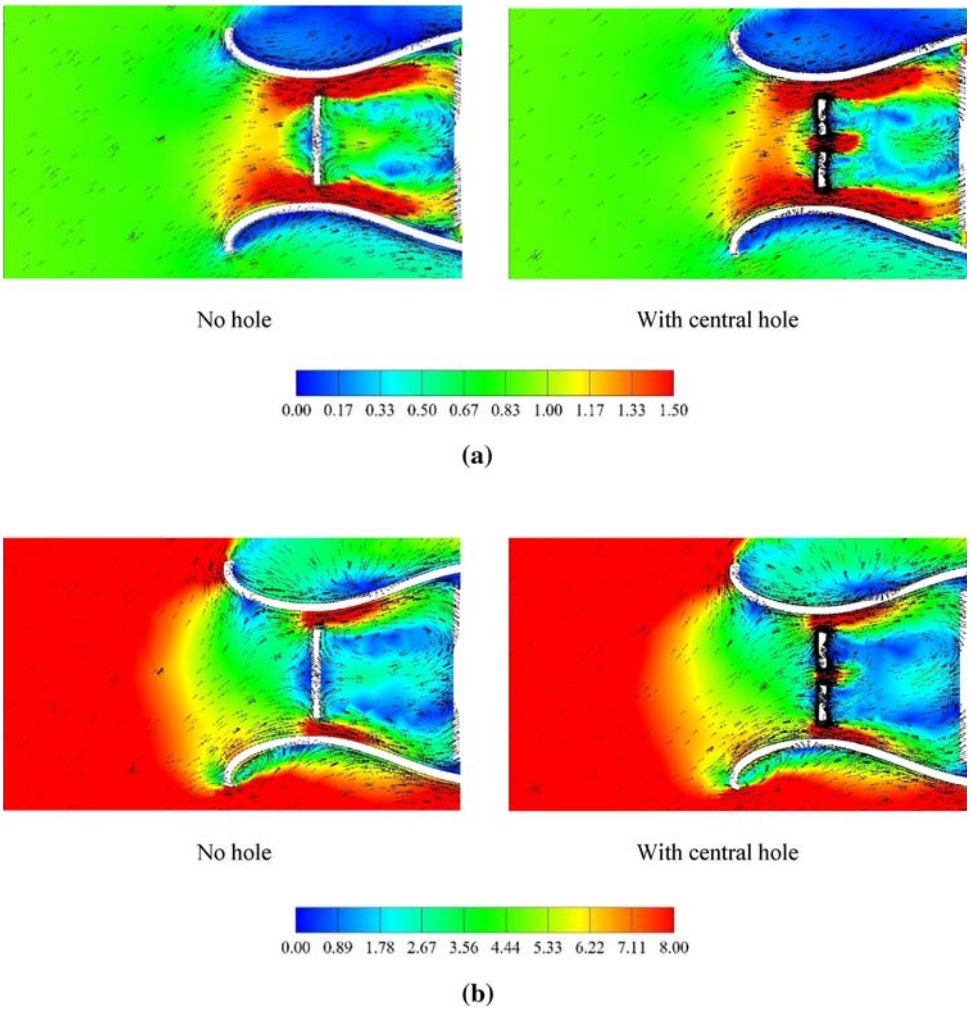

Figure 22. Contours of velocity magnitude along with velocity vectors in the vertical azimuthal plane. (a) V_∞ = 1 m/s and (b) V_∞ = 12 m/s. The angle of attack is 45° in all these cases.

increase with an increase in forward velocity. The large values of τ_w are due to the ram effect. This should increase the sensitivity of the chemical sensor. An important observation is that τ_w values do not depend on the angle of attack. The air suction duct design is successful and maintains the effectiveness of the disc even at an angle of attack as large as 45°.

The τ_w values plotted in figure 19 represent only an average value. But what matters is the distribution of the shear stress. This was studied through the contours of axial velocity at various stations in the air suction duct and is shown in figure 20 for forward velocity of 1 m/s and angle of attack of 45°. Station x = 0 mm is at the inlet of the duct and station x = 7 mm is ahead of the sensor disc by 3 mm. It may be recalled that the sensor disc is located at x = 10 mm. In the inlet plane the axial velocity is symmetrical about the vertical axis with high velocities at the lower portion since the freestream velocity vector is in the vertical plane. We clearly see a lack of axisymmetry. However, at x = 5 mm, remarkably, there is a tendency towards axisymmetry and a decrease in the boundary layer thickness. Also, there is an increase in average velocity. These are due to the decrease in cross-sectional area of the converging section of the duct. These trends are seen further from the contours at x = 7 mm.

It may be added that a sharp decrease in cross-sectional area in the converging section and also especially the presence of a through hole in the sensor disc at the centre quickly drive the flow towards axisymmetry as desired. We see this effect of the wall shear stress distribution on the front wall of the sensor disc in figure 21 for three freestream velocities 0.1, 6 and 12 m/s for angle of attack = 45°.

Contours of velocity magnitude along with velocity vectors are shown in the vertical azimuthal plane in figure 22. The effective turning of the flow by the converging section of the nozzle is seen for both the cases of V_∞ = 1 m/s in figure 22(a) and V_∞ = 12 m/s in figure 22(b). There is a stagnation area only in the upper part of the nozzle but, as was seen in figure 19, the velocity field

becomes axisymmetric quickly. Further, we see clearly in figure 22 how the central hole makes the flow more uniform on the face of the disc.

8. Conclusions

An efficient air suction system meant for a chemical sensor to detect small traces of gases and vapours has been designed. The chemical sampling system consists of an air suction system with a miniature axial flow fan and a chemical sensor. The device is meant to be mounted on a micro aerial vehicle so that large areas can be surveyed quickly. The presence of a fan enables sensing when the vehicle is hovering or has perched. The device has been designed for high aerodynamic sensing efficiency and low weight around a miniature fan after testing its aerodynamic efficiency.

A suitable miniature fan was selected and its performance was evaluated computationally. An air suction system concept was arrived at around this fan with a converging-diverging geometry with the sensor disc being at the throat. The location and orientation of the sensor disc and further it having a central hole improved mass transfer of the gas molecules to be detected from air to the sensor element as supported using Reynolds analogy. Thus, the air suction duct apart from protecting the sensor disc enhances the aerodynamic sensing efficiency. Due to the careful design of the converging part of the duct and the presence of a hole in the sensor disc the flow is seen not to separate but to reach axisymmetry and high wall shear stress on the disc face even at high flow angles of attack.

It may be concluded that a good low weight design of the air suction system has been achieved to give good aerodynamic performance even under extreme flow conditions that may be caused by MAV manoeuvre or cross winds. An application has been filed to patent this work in India [24].

Acknowledgements

We thank the Department of Science and Technology (DST), New Delhi for funding this project; the Programme Office, National Programme on Micro Air Vehicles (NPMICAV), Aeronautical Development Establishment, Bengaluru for sanctioning and monitoring the project; and the National Design and Research Forum (NDRF), Bengaluru of the Institution of Engineers (India) for coordinating the project.

Nomenclature

D_1, D_2, D_3, L_1, L_2	dimensions of the sensor duct (mm) (see figures 8 and 15)
d	diameter of the hole in the sensor disc plate (mm)
L	total length of the air suction duct = 30 mm
p	pressure (Pa)
Q	volumetric flow rate (lpm)
T	torque (N-m)
v	velocity (m/s)
V_∞	velocity of the MAV carrying the air suction device (m/s)
z	fan axis and also flow direction

Greek symbols

α	angle of attack of air suction device with freestream (deg)
ρ	density of air (kg/m^3)
τ_w	wall shear stress (Pa)
ω	fan rotational speed (rad/s)

References

[1] Soderman P T, Hazen N L and Brune WT 1991 Aerodynamic design of gas and aerosol samplers for aircraft. *NASA TM* 103854

[2] Perajarvi K, Lehtinen J, Pollanen R and Toivonen 2008 Design of an air sampler for a small unmanned aerial vehicle. *Radiation Protection Dosimetry* 132: 328-333

[3] Pollanen R, Toivonen H, Perajarvi K, Karhunen, T, Ilander T, Lehtinen J, Rintala K, Katajainen T, Niemela J and Juusela M 2009 Radiation surveillance using an unmanned aerial vehicle. *Applied Radiation and Isotopes* 67: 340-344

[4] Settles G S and Kester D A 2001 Aerodynamic sampling for landmine trace detection. *SPIE Aeroscience* 4394, Paper 108

[5] Settles G S 2005 Sniffers: Fluid-dynamic sampling for olfactory trace detection in nature and homeland security. *J. Fluids Eng.* 127: 189-217

[6] Sharan M and Gopalakrishnan S G 1997 Bhopal gas accident: A numerical simulation of the gas dispersion event. *Environmental Modelling & Software* 12: 135-141

[7] Ho C K, Itamura M T, Kelley M and Hughes R C 2001 Review of chemical sensors for in-situ monitoring of volatile contaminants. *Sandia Report* SAND2001-0643

[8] Siadat M, Losson E, Ahmadou D and Lumbreras M 2014 Detection optimization using a transient feature from a metal oxide gas sensor array. *Sensors & Transducers* 27: 304-346

[9] Liu H, Zhang L, Li K H H and Tan O K 2018 Microhotplates for metal oxide semiconductor gas sensor applications – Towards the CMOS-MEMS monolithic approach. *Micromachines* 9: 1-24

[10] Holman J P 2009 *Heat Transfer*. 10th edn. New York: McGraw-Hill

[11] Bejan A 2013 *Convection Heat Transfer*. 4th edn. New Jersey: Wiley

[12] Judy J W 2001 Microelectromechanical systems (MEMS): fabrication, design and applications, *Smart Materials and Structures* 10: 1115-1134

[13] Wallis R A 1983 *Axial Flow Fans and Ducts*. New York: John Wiley

[14] Eck B 1972 *Fans: Design and Operation of Centrifugal Axial Flow and Cross Flow Fans*. Oxford: Pergamon

[15] Bleier F P 1997 *Fan Handbook: Selection Application and Design*. New York: McGraw-Hill

[16] Quin D and Grimes R 2008 The effect of Reynolds number on microaxial flow fan performance. *J. Fluids Eng.* 130: 101101

[17] Kearney D, Grimes R and Punch J 2009 An experimental investigation of the flow fields within geometrically similar miniature-scale centrifugal pumps. *J. Fluids Eng.* 131: 101101

[18] Walsh P A, Walsh E J and Grimes R 2010 Viscous scaling phenomena in miniature centrifugal flow cooling fans: Theory, experiments and correlation. *J. Electron. Packag.* 132: 021001

[19] Grimes R, Davies M, Punch J, Dalton T and Cole R 2001 Modeling electronic cooling axial fans. *J. Electron. Packag.* 123: 112-119.

[20] Lin S-C and Tsai M-L 2010 An integrated performance analysis for a small axial-flow fan. *J. Mech. Eng. Sci.* 224: 1981–1994

[21] Lin S-C and Tsai M-L 2011 An integrated study of the design method for small axial-flow fans, based on the airfoil theory. *J. Mech. Eng. Sci.* 225: 885–895

[22] Deshpande M D, Sivapragasam M and Umesh S 2014 Air suction system for chemical sensor for MAV application. *Compendium on Advances in Micro Air Vehicles in India*, National Design and Research Forum, Bengaluru

[23] Celik I B, Ghia U, Roache P J, Freitas C J, Coleman H and Raad P E 2008 Procedure for estimation and reporting of uncertainty due to discretization in CFD applications. *J. Fluids Eng.* 130: 078001

[24] Deshpande M D, Sivapragasam M and Umesh S 2015 Apparatus for enhancing aerodynamic sensitivity of a chemical sensor, Indian patent application number: 7093/CHE/2015